Open access • Journal Article • DOI:10.1103/PHYSREV.130.1505

Bremsstrahlung from proton bombardment of nuclei — Source link

David Cohen, Burton J. Moyer, Harlan C. Shaw, Charles N. Waddell

Published on: 15 May 1963 - Physical Review

Topics: Bremsstrahlung, Proton, Photon energy, Neutron and Photon

UCRL-3230

UNIVERSITY OF CALIFORNIA
Radiation Laboratory
Berkeley, California

Contract No. W-7405-eng 48

BREMSSTRAHLUNG FROM PROTON BOMBARDMENT OF NUCLEI

David Cohen

December, 1955

Printed for the U. S. Atomic Energy Commission

TABLE OF CONTENTS

BREMSSTRAHLUNG FROM PROTON BOMBARDMENT OF NUCLEI

David Cohen

Radiation Laboratory, Department of Physics
University of California, Berkeley, California

December, 1958

A. General Background

Bremsstrahlung, or braking radiation, may be defined as the electromagnetic radiation emitted by a free charged particle when it undergoes acceleration with respect to the observer. A well-known example of this phenomenon is the continuous part of the X-ray spectrum, produced when free electrons in the kilovolt energy region strike and penetrate a metal target and hence undergo deceleration.

In the experiment to be described, various targets were bombarded with protons in the 40-140 Mev region, and the γ-ray spectra were detected and analyzed. Under the assumption that the γ-rays originated from the deflected protons, the purpose of the experiment was to obtain information about the nature of the nuclear interactions through which the protons suffered changes of state.

In brief, the experimental method of investigation consisted of bombarding various internal targets with protons in the synchrocyclotron, and viewing these targets with a pair spectrometer. The bombarding energy was kept below the neutral meson production threshold so that photons from neutral meson decay would not distort the

bremsstrahlung spectrum.

Although some experimental work had already been done on proton bremsstrahlung[1], it was felt that the application of a different and more refined technique of pair spectrometry might make a more complete study worthwhile. In particular, the E-dependent and energy dependent spectra were investigated more fully. Comparisons of experimental results and theoretical conclusions with this previous work will be made later.

There are a number of possible avenues that one may explore in attempting to predict theoretically the nature of these γ-ray spectra.

The classical electrodynamics is useless in this case. It is clear that for the nuclear interactions which can possibly be involved the detected wave length of the radiation is comparable with or shorter than the diameter of the region in which the proton may be supposed to be effectively located during its change of state. This is the well-known criterion for the breakdown of classical electrodynamics in such radiation processes, and the classical approach must therefore be abandoned.

Various authors have attempted to predict the proton bremsstrahlung spectra using the quantum electrodynamics.[2,3,4] Simon, Ashkin and Marshak assume single proton-nucleon collisions, and predict spectra based on meson and phenomenological nucleon-nucleon interactions. The phenomenological treatment is discussed in D(3) . Kursunoglu assumes only a proton-nucleus interaction by

means of a complex square-well potential, but at the present time accurate quantitative results of this calculation are not available due to the vast computation work involved. A tabular summary of these predictions is given in figure 14, and figures 12 and 13 give various graphical analysis.

The nucleon-nucleon collisions which contribute to the radiation are only of the p-n type, since the quantum electrodynamics shows there can be no electric dipole radiation from p-p collisions. One of the possible results of this experiment would be the test of the purity of the p-n or proton-nucleus collision processes.

On simple theoretical grounds one would expect that the pure p-n collision picture should not be perfectly valid for proton bombarding energies of 140 Mev and less, since the de Broglie wavelength of a 140 Mev proton is about 3×10^{-13} cms., which is slightly less than the diameter of the Be^{9} nucleus. Be was the target most carefully dealt with in this series of experiments. However, in view of the fact that at this time no comprehensive, precise model of the nucleus is in existence, one must resort to perhaps artificial and restricted models which have been useful in this bombarding energy range. The nucleon-nucleon collision picture has been shown to be frequently adequate at bombarding energies of 90 Mev and greater. The target nucleus, in the simplest case, is viewed as a degenerate Fermi gas of nucleons. This is a rough first approximation from which one easily finds a nuclear momentum distribution. This distribution for low Z nuclei has been found to differ

significantly from the experimental distribution results, and hence cannot be used with any accuracy and validity for the lower Z targets.

For such lower proton bombarding energies, where the proton de Broglie wavelength is appreciably greater than the diameter of the struck nucleus, in general reactions are described through the compound nuclear model[5]. This can be justified from several points of view. On the wave-mechanical picture, the bombarding proton "cannot distinguish any nuclear structure" and therefore interacts with the nucleus as a whole. On the more classical picture, the bombarding proton is travelling at a lower speed, spends more time in the nuclear region, suffers more collisions because the total p-n collision cross section varies inversely as the energy, and so the nuclear system has a high probability of readjustment to a compound nuclear state; after the proton has undergone enough collisions it will not have enough energy to escape the nuclear well, and is captured. It would appear, therefore, that a theoretical description of the bremsstrahlung in this energy region would be difficult. If the bombarding energy is low enough so that only the Coulomb field interaction is present, the bremsstrahlung cross sections may be predicted from the analogous electron case, with proper correction for the mass difference.

In the energy region too high for compound nuclear consideration and too low for pure p-n collision analysis (for example about 20-80 Mev bombarding energy for

Be), where the bombarding proton has a good probability of escape from the struck nucleus, the most direct theoretical approach for the prediction of the bremsstrahlung effects would be consideration of proton collisions with a nuclear potential well. The well is described in terms of real and imaginary parts, since there will be secondary proton emission. Such an approach was undertaken by Kursunoglu[4].

The general methods used in the nucleon-nucleon collision picture were proposed by Serber[5], enlarged upon by several authors[6,7], and were used to explain several nuclear phenomena[H], among them the high-energy spallation reactions[8]. These methods consist of following the paths of a number of bombarding nucleons in the nuclear region as they suffer single and multiple collisions with the target nucleons of various momenta; due to the element of randomness involved, the Monte Carlo method can be used, and a recent attempt has been successful in an application to (p,pn), (p,2p) and (p,2n) reactions[9].

[H]A full discussion with appropriate references of this type of problem is presented on pages 30, 142, etc. of E. Segre "Experimental Nuclear Physics", Vol. II.

The mean free path of the bombarding nucleon in nuclear matter is given by

$$\lambda = \frac{1}{\bar{\sigma}\rho_t}$$

where $\bar{\sigma}$ is the average total cross section[m] for the nucleon-nucleon collisions and ρ_t is the total nucleon density, so that for 100 Mev protons the mean free path is about 1.3 x 10^{-13} cms., or somewhat less than the radius of the Be^9 nucleus; for 140 Mev protons the mean free path is about equal to the Be^9 nuclear radius. These facts allow a great simplification in the theoretical application to the Be^9 nucleus, for they show that for 140 Mev bombarding protons only single nuclear collisions need be considered for an adequate approximation, and the Monte Carlo method may be discarded in this case. For larger nuclei, such as Cu, multiple nuclear collisions are more probable than single collisions, and a theoretical spectrum prediction must involve a collision sampling process, such as the Monte Carlo method.

The case for larger nuclei is further complicated by nuclear events which compete with the (p,p) process. For example, for a nucleus of mass 64, Meadows[9] has shown

---

m Values for $\bar{\sigma}$ were chosen for the bombarding energies of interest by using the experimental values from references 15 and 16 of Meadows'[9] paper.

theoretically that the probability for the (p,2p) event is comparable to the (p,p) probability, which is in agreement with experimental results. The energies involved with the outgoing nucleons of these competing reactions are such that a significant contribution to the photon spectrum may be expected.

These considerations show that the 140 Mev proton bombardment of Be^9 is the least complex case in these experiments for a theoretical nucleon-nucleon analysis. This case was given detailed consideration and interpretation, while all other spectra were treated in a more qualitative fashion.

The experiments here described also set limits to or measure the cross section for the reaction $p+n \rightarrow d+\gamma$ inside the target nuclei. A simple analysis of this reaction shows that for stationary target neutrons and fixed detector geometry the resulting photons are confined to a narrow spectral region, where the mean photon energy is about one-half the proton bombarding energy in the laboratory system. For moving target nucleons this narrow spectral region is somewhat broadened. If the photon flux from this reaction is comparable in magnitude to the bremsstrahlung photon flux in the same spectral region, a "hump" should be seen superimposed on the more slowly-varying bremsstrahlung spectrum.

B. Experimental Technique

(1) Pair Spectrometry in General

The essential principles and techniques of pair spectrometry have been known and used for some time[10], and

will here be only briefly reviewed. A photon of energy greater than 1.02 Mev, in passing through a metallic foil or "converter", may undergo pair production. The resulting electron-positron pair, in a uniform magnetic field, proceed with opposite circular orbits to detection areas, where charged particle detectors record the coincident passage of the pair. (See figure 1). For the case where the detectors and converter lie on the same straight line perpendicular to the γ-ray direction, the pair spectrometer is called the 180° type, and a simple analysis shows that

$$W = \sqrt{m_0^2 c^4 + p_{(+)}^2 c^2} + \sqrt{m_0^2 c^4 + p_{(-)}^2 c^2} .$$

If $pc \gg m_0 c^2$ then

$$W \approx p_{(+)} c + p_{(-)} c,$$

and for a charged particle in a magnetic field

$p = Be\rho$, so that

$$W \approx Bec(\rho_{(-)} + \rho_{(+)});$$

where W is the photon energy, B is the magnetic flux density, e is the electronic charge, c is the velocity of light, and $\rho_{(-)}$, $\rho_{(+)}$ are the radii of curvature of the electron and positron, respectively. Thus for a given magnetic field, the γ-ray energy is uniquely determined by the electron-positron separation on the line. The pair spectrometer used in this research was of the 180° type.

(2) Design and Use of the 180° Pair Spectrometer

The pair spectrometer was set up at the 184" synchrocyclotron outside the concrete shielding, and viewed internal targets from about 45' through the shielding holes

and tank ports. (See figure 2).

The primary consideration in the general design of the spectrometer was to minimize the energy loss and scattering of low-energy pairs in passing through the converter so that continuous γ-ray spectra in the 10-180 Mev interval could be detected and analyzed without the insertion of severe corrections. The spectrometer was designed, then, to use relatively thin converters; e.g., .003" tantalum foil. Tantalum was chosen because of its relatively high Z. A high Z material was justified because:

(a) the pair production (desirable process) cross section is proportional to $\frac{Z^2 t\rho}{A}$;

(b) the Compton effect (undesirable process) cross section is proportional to $\frac{Zt\rho}{A}$;

(c) the mean scattering angle $\sqrt{\overline{\phi^2}}$ (undesirable process) is proportional to $Z\sqrt{\frac{t\rho}{A}}$;

(d) $\left(\frac{dE}{dx}\right)_{ion.}$ (undesirable process) is proportional to $\frac{Zt\rho}{A}$;

(e) $\left(\frac{dE}{dx}\right)_{rad.}$ (undesirable process) is proportional to $\frac{Z^2 t\rho}{A}$;

where t, ρ, and A are the target thickness, density, and atomic weight respectively.

Since the $\left(\frac{dE}{dx}\right)_{rad.}$ and radiation straggling effect were not serious for continuous spectra determinations with tantalum converters of .003" (or thinner), and the mean scattering angle was of importance in both horizontal and vertical scattering, a high Z material was chosen. It was also found that Compton electrons, under some conditions of

detection, were bothersome (accidentals, blocking of geiger tubes) and it was useful to have their relative effect minimized.

With thin converters it was necessary to evacuate the air in and preceding the converter region in order to eliminate pair production in air and the resulting detectable spectrum distortion. Ten geiger tubes on each side, symmetrically placed with respect to the converter, detected the electron pairs. (See figure 3). Subsequent electronics analyzed the spectrum.

(3) Physical Arrangement in Detail

The pair magnet was originally designed by H.F. York and Paul Hernandez for general high energy pair spectroscopy at the synchrocyclotron. The pole tips formed the top and bottom of the enclosed pair chamber, and the entire chamber was removable. The tips were of 1½" magnetic steel, with a 3½" separation. The chamber sides were of stainless steel, and all joints were welded vacuum tight. Wherever possible the chamber was lined with aluminum plate to reduce scattering from the top, bottom, and sides into the geiger tubes. (See figure 4). The converters were mounted on wire frames which were controlled from the outside by means of springs, strings, and rods through Wilson seals. The two windows in front of the geiger tubes were covered by .007" aluminum foils, and were the best compromise between strength for maintaining vacuum and small electron scattering angle into the geiger tubes. A 6' long, 4" diameter brass pipe completed the vacuum system. An 18" collimator with sides of brass and top and bottom of magnetic steel was built into this

pipe at the entrance end. Heavy alnico magnets and steel yoke around the pipe provided the necessary magnetic field inside the collimator for clearing away pairs formed in the end foil (.007" Al.) and the collimator.

The various internal cyclotron targets were mounted in a copper clamp at the end of a thin copper bar of 6" length which was extended radially into the cyclotron tank and the entire unit was bolted to the water-cooled end of the "hollow" probe. (See figure 5). Constantan wires were soldered to both ends of the copper bar, and the resulting thermocouple allowed measurements of beam power dissipated in the target and hence a calculation of beam current necessary to absolute cross section measurements.

(4) Pair Spectrometer Concepts in Detail

(a) The Matrix Principle

The electronic aspects of this principle had been developed some 6 years ago, and were last used in its present form by Crandall and Hoyer.[11] Since pairs may originate anywhere in the extended converter, and all types of energy splittings are possible, it can be seen that pairs originating from a particular photon may end up in any one of a number of pairs of geiger tubes; i.e., a particular pair of geiger tubes determines the photon energy only by virtue of the distance between them. Referring to figure 6, it is apparent that if geiger tube outputs determine the rows and columns of the matrix as indicated, the lines parallel to the vertical diagonal are monoenergetic in nature (to a resolution ΔW determined by geiger tube width and magnetic field). Each vertical line,

then, refers to a particular γ-ray energy within resolution ΔW, and the γ-ray energies of the various coincidences can be neatly sorted by the electronics of such a matrix. Henceforth, these vertical lines will be designated as "energy channels". The channel energies are uniquely determined by the magnetic field for a given tube spacing.

(b) Channel Efficiencies

The efficiency of each channel in recording the number of photons of appropriate energy which are directed at the converter depends on a number of considerations. To derive the value of the efficiency of each channel it is useful to trace the events which may occur to a number of photons of various energies which are directed at the converter.

The first phenomenon encountered is that of pair production in the converter. The probability of one of these photons producing a pair in the converter depends on the total pair production cross section, which is a function of the target Z, and the photon energy. Bothe and Heitler have theoretically derived this cross section on the basis of the Born approximation, and a particularly useful form of the cross section is given by Rossi and Greisen.[12] Since the conditions for the validity of the Born approximation in the energy ranges considered here is that $\frac{2\gamma Z}{137} \ll 1$, it is expected that the Bothe-Heitler cross section may be a poor approximation for increasing Z. Experiment[13] shows that this is indeed the case, (for tantalum the error is of the order of 10%) and the pair-production cross section here used

contains the suitable empirical corrections. The total pair-production probability in the converter is then $N_0 \frac{\delta}{A} t \Phi(W,Z)$, where $N_0 \frac{\delta}{A} t$ is the number of nuclei per unit area, and $\Phi(W,Z)$ is the corrected total pair-production cross section for the converter material, of atomic number Z and photon of energy W.

For a given setting of the magnetic field of the pair spectrometer, only those pairs in the appropriate energy range have a chance of coincidence detection by one of the 19 channels. Other energy pairs may split in such a way so that one member of the pair may pass through a geiger tube on one side or the other, but the other member will fall inside or outside the geiger tube region on the opposite side. The production of Compton electrons, (which is not insignificant below 20 Mev photons) and photonuclear events in the converter do not produce pairs for coincident detection. The production of electron-positron pairs by the photons in the field of the atomic electrons[14] is another effect to be considered; calculations show that for tantalum the probability is of the order of 1% of the nuclear analogue, and hence this effect can be neglected.

One or more of the following four events may now occur to a pair of appropriate energy.

One or both members of the pair may be vertically scattered into the top or bottom of the pair chamber, and be lost by penetration into the aluminum plate. (For aluminum this is far more probable than backscattering into the geiger tube region). This vertical scattering loss will be

dealt with more fully in later sections.

One or both members of the pair may pass between the counting areas of neighboring geiger tubes and are lost for detection. This "dead" area is evaluated by geometric considerations and by a simple analysis of the effective geiger tube areas which involves the cylindrical form of the tubes.

The next type of event involves the characteristics of the division of available kinetic energy between the members of a pair. All types of splitting are possible, and a typical splitting probability curve is shown in figure 6. The total pair production cross section is proportional to the area under this curve. Only a certain range of splitting can be received for a particular channel; this range depends only on the geometry of the converter and geiger tube arrangement, and is independent of the magnetic field setting. If the splitting curve was flat, then it is clear that this geometric efficiency is the ratio:

$$\frac{\text{actual geiger tube area for this channel}}{\text{total area in the detector plane ideally available for pair particle traversal at this energy}}$$

However, since the curve is not flat, the precise determination of the efficiencies involved is complicated and involves some tedious numerical work. In the appendix (1) a full derivation is given for the channel efficiencies, and approximations are made in order to obtain simple, usable results. Perhaps the most significant approximation is considering the splitting curves as flat. In practice the

height of this horizontal line was chosen to correspond to $\eta = .3 = .7$ on the actual curves; this was considered a good averaging, and allowed rapid calculation of the efficiency.

The fourth possible event is actual coincidence detection.

The absolute channel efficiency is then approximated by (pair production probability for a particular converter and energy) X (fraction of pairs surviving loss by vertical scattering) X (fraction of coincidences surviving loss by passage between geiger tubes) X (geometric efficiency).

(c) Geiger Tubes

The geiger tubes would have been considered ideal if they all had the same area and counting efficiency, and if their characteristics remained constant throughout many months. Unfortunately, neither of these conditions existed, and some time was spent in overcoming the resulting difficulties.

It is clear that if, say, the inside geiger tube on one side had, say, 30% greater area than all the other 19 tubes (which may here for the sake of argument be considered as a "matched set" of 19), then appropriate corrections must be inserted in the channel efficiencies. Since this inside tube does not appear in the 11th channel, it may be called a "good" channel, and with respect to this channel a correction of 30% must appear in the first channel, 15% in the second channel, etc. If the 30% changed after some months to, say, 40%, then ideally these corrections must all be changed,

with resulting numerical tedium.

Methods and ideas were finally evolved so that none of these geiger tube efficiency corrections were necessary. To deal with the problems involved it was essential that a beam of particles be found which was uniform over a large area in order to test the counting efficiency of the tubes. Such a beam was furnished by the cosmic rays, which have an energy and areal spread quite suitable for testing the tubes. The tubes were eventually tested by being placed in a horizontal plane on a table and allowed to count during the night so that the accelerator radiation background was not present. Each set of 10 tubes was contained in its pair spectrometer mounting, and during succeeding nights these mountings were rotated in various ways so that variations (due to nearby structures) of the cosmic-ray intensity along the surface of the table would be compensated for by suitable averaging. The electronics involved in recording the cosmic-ray counts consisted of the available pair spectrometer counting and recording equipment, and the results appeared on the geiger registers. (See section (5)).

By means of such testing it was possible to find a set of tubes which had counting efficiencies matched to within 8%, and which did not change in counting characteristics over the many nights of testing. Occasionally, of course, a tube might radically change characteristics during an actual cyclotron run, and was replaced by a suitably tested spare.

The maximum 8% efficiency difference between

tubes may be shown to produce no significant resulting spectrum distortion if the spectra are viewed with suitable magnetic field settings in the spectrometer. That is, if the energy ranges corresponding to the different magnetic field settings overlap one another for a given spectrum, then the geiger tube efficiency errors tend to be minimized, since a particular photon energy will be associated with different geiger tube arrangements for each magnetic field setting.

(d) Vertical Scattering

An appreciable number of electrons will not reach the geiger tubes because of vertical scattering into the pole tips. If it can be shown that at any vertical line (i.e., for any given electron path radius) in the geiger tube region the fraction of electrons lost from the sensitive segment of this line by vertical scattering is a constant, it then follows that there is no resulting spectrum distortion. In the appendix (2) it is proved that certainly at least to a first approximation this is true; and by use of thin convertors and proper matching of spectra from different magnet field settings this second order distortion is made negligible. The constant fractional loss, however, is not negligible and is determined both theoretically and empirically.

(e) Horizontal Scattering

The focussing properties of 180° circular orbits are well-known, so that horizontal scattering results in no spectrum distortion, if the scattering angles are small. Orbits were experimentally investigated by the "wire orbit" method. (See field calibration section).

(5) General Description of Electronics

Figure 7 outlines the general electronic arrangement. Each of the 20 geiger tubes was followed by a pulse-forming unit, designed by Charles Waddell, which transformed the rising portion of a geiger pulse into a one microsecond square pulse. The bias on each of the 20 thyratrons was controlled by means of a potentiometer, and allowed the firing voltages to be lined up with a pulser. In this way all thyratrons fired at the same point on the rise of the geiger tube pulses and would not distort succeeding coincidence characteristics. The thyratrons in general fired at a small fraction of the maximum geiger voltage, so that the firing voltages were not critical and electronic "jitter" was effectively eliminated.

If the geiger tube events occurred so that only one tube on each side fired within a time range of .8 microseconds, then this was called a "true" β-ray coincidence and a gating pulse (from the lower half of the electronics in figure 7) allowed the modified geiger pulses to pass through the 35 channel gated amplifier. Twenty channels of the 35 channel amplifier were used; one channel for each geiger tube. These amplifiers served the purpose of amplifying the modified geiger pulses into 20 millisecond pulses to suit the current requirements of turning over the subsequent channel registers. One bank of ten amplifiers fed the rows of the 10 x 10 matrix, the other bank fed the columns. The matrix proper consisted of a square of 100 6SJ7's. Along any row all suppressor grids were tied together, along any column all control grids were tied together, and along any

diagonal all plates were tied together. The tubes normally operated at cutoff, and a coincidence on any row and column would allow plate current to flow in the tube situated at the junction of the row and column. The signal was transmitted along the diagonal, amplified, and operated a channel register which referred to this particular diagonal. The geiger registers indicated which particular two geiger tubes had fired, and primarily served as monitors allowing rapid spotting of any ineffective geiger tube.

If two separate coincidences were allowed to arrive at the matrix separated by, say, one millisecond, then it can be seen that as many as four registers may turn over, giving two false counts. This sort of mixing is eliminated by the dead-time circuit, which only passed gating signals to the 35 channel amplifiers if they were separated by at least 15 milliseconds.

The most critical section of the electronics is situated in the lower half of figure 7. This is the section in which the coincidence characteristics of the geiger pulses are analyzed. It can be seen that two cables, labeled L and R, feed this lower section. Each cable carries all outputs from each bank of 10 geiger tubes, the left bank and the right bank. The thyratron outputs on each bank were mixed by means of cathode followers to yield these added left and right bank "singles". The unit labeled "amplifiers and anti circuit" served two purposes. The first was to amplify these added pulses so that their heights are suitable for operating the subsequent adjustable gate-forming units. The one microsecond pulse width was unaltered. The second purpose was to

determine, by means of a Germanium diode system, if triple-coincident events were present and to transmit a pulse for any such event. Triple-coincident events were defined as events where three or more geiger tubes fired within .8 microseconds of each other, involving both banks of geiger tubes. For example, if two geiger tubes on the left side fired in coincidence with one geiger tube on the right side, such events were not permitted to enter the matrix, by the action of the "anti" circuit. There were several reasons for monitoring such events. It was possible, by means of such monitoring to investigate the kinematics of the pulse-producing particles in the geiger tube region, so that geiger-to-geiger scattering, and other such events, could be exposed if they took place. Also, the frequency of these events with the rise and fall of the cyclotron beam level gave information about accidentals from Compton and pair electrons from the converter and the general radiation background.

The left bank, right bank, and anti-pulses were then lined up with respect to one another and the arrival time of the modified geiger signals through the delay lines into the 35 channel amplifier by means of the three adjustable gate-forming units preceding the 10 channel quad mixer. (This mixer is simply a multiplex coincidence system in which any combinations, up to quadruple coincidence, may be selected out of ten input channels). The left bank added pulses were also fed into an auxiliary adjustable gate-forming unit which delayed these pulses by 5 microseconds. These delayed pulses, when mixed with the added right pulses, allowed monitoring of the purely accidental coincidence rate. The pulses from all

four gate-forming units were adjusted in width so that the various coincidences, which were determined in the 10 channel quad mixer, were of .8 microseconds resolving time.

The 10 channel quad mixer was adjusted so that it was used as a coincidence unit which determined events as labeled on the four subsequent scalers. Certain scalers were disabled with a 120 microsecond gate triggered by the cyclotron r.f. pulse, and thus monitored only the "off-beam" counts. The gated scaler which recorded the true coincidences of particles of a single pair, labeled L + R - A, also sent out the gating pulse, through the dead-time circuit and a variable-delay, variable gate (V.D.V.G.) unit, to the 35 channel amplifiers.

In general, the electronic arrangement was designed to use as much available equipment as possible, hence was somewhat more involved than was really necessary. However, it was found that satisfactory operation was obtained if frequent, general tests were made with a pulser substituting for the raw geiger pulses. Eventually a semi-automatic pulsing tester was evolved which tested all phases of the electronics in the order of 20 or 30 minutes. The monitoring scalers and registers were so arranged that any bad electronic tubes along the line could be detected without having wasted much beam time during an actual run.

(6) Magnetic Field Calibrations

The magnetic field distribution and field strength as a function of magnet current were calibrated by three independent methods. It was of primary importance

that the properties of the field distribution be such that a plot of electron energy vs. distance along line of centers of the geiger tubes yield a straight line for an electron leaving the convertor region. If no straight line results, then the matrix principle is not applicable.

(a) Floating Wire Technique

For a current-carrying wire in a magnetic field, where no forces on the wire other than the amperian force and tension are acting, it can be shown that

$$\frac{T}{I} = B\rho$$

where T is the tension
I is the current,
B is the magnetic flux density
ρ is the radius of curvature,

but since for an electron

$$B\rho = \frac{p}{e}$$

where p is the momentum
e is the electronic charge

and if $\beta \approx 1$ then

$$p \approx \frac{E}{c}$$

where E is the total or kinetic energy;

so that

$$\frac{T}{I} = \frac{E}{ec}.$$

Thus, by suspending a wire in the median plane of the pair chamber, varying the current, tension and exit angle from the converter, it was possible to plot orbits, check the 180° focussing properties, and obtain a general picture of the magnetic field properties.

(b) Proton Probe Measurements

The magnetic field at various points in the

pair chamber was measured with a proton spin-resonance probe, and the resulting magnetic field distribution allowed the plotting of orbits of the pairs as a function of current through the pair magnet.

(c) Calibration with Known γ-ray Line

The well-known[15] 17.6 Mev γ-ray line from Be^{8*} was generated by 440 Kev protons on Li^7 at the Van de Graaf generator, and the pair spectrometer was moved to the target region in order to detect this line. In spite of low counting rates, the line was suitably detected and analyzed.

The agreement between all three calibrations was very good, and the results of the floating-wire measurements showed that the matrix principle was applicable.

(7) Evaluation of the Accidental Spectra

During some of the runs the percentage of coincidences which were accidental in origin was found to be as high as 20%. In order to determine the apparent photon spectra due to these accidental coincidences, as a function of target material and magnet current, the 20 amplifiers were gated with a wide (about 100 microseconds) "on-gate" derived from a frequency-sensitive device sampling the cyclotron R.F. and initiating the gate at that frequency for which the beam will emerge from the cyclotron. Since only a small percentage of geiger counts had their origin in γ-ray pairs, the registers in this case rapidly accumulated the accidental spectra. These spectra were then properly subtracted from the spectra accumulated under proper running

conditions.

The accidentals had their origin in Compton electrons from the converter (especially at lower magnet currents), the secondary products inside the chamber from target neutrons, the general radiation background, and from fragments of two or more independent pairs.

C. Evaluation of the Data

The spectra from the different magnetic field settings, suitably corrected for accidentals, were plotted independently of one another. (See figures 8 and 9). In plotting these spectra absolutely, some care was given to the use of the target thermocouple readings. In particular, it was necessary to know how much heat was being lost from the target by radiation. Since $\frac{\text{emissivity}}{\text{conductivity}}$ in carbon is much higher than in the metals, a large radiation loss relative to the metals was to be expected. The problem was solved by plotting thermal rise and decay curves for different targets bombarded to various temperatures. It was noticed that after a relatively low beam was turned off, the thermal decay curve was an exponential from a metal target. Deviations from the exponential were found at initially higher target temperatures, this deviation being especially marked with carbon. By solving for various constants in standard thermal exponential equations from the decay and rise curves, it was possible to evaluate roughly the radiation loss. This loss was small in metals, but of the order of 50% at times in carbon.

A more accurate method of dealing with the

radiation loss was based on the assumption that the left-bank and right-bank singles rate was directly proportional to the beam level up to the point where "blocking" became appreciable in the geiger tubes. Thus, at low beam levels where the radiation loss from the target was not appreciable, the singles rate could be calibrated for absolute beam level from the thermocouple reading. At higher beam levels but still short of blocking conditions, the singles rate then served as an adequate monitor for absolute beam levels.

Figures 8 and 9 show that the various spectra overlap and match quite nicely. Since wide variations of target temperatures were attained in gathering these spectra, the suitable matching indicates that the thermal radiation was adequately dealt with.

The errors shown on the curves are the "probable errors" from statistics.

D. Final Results

(1) General Discussion

Figures 8, 9, 10 and 11 show the experimental results. The points for the various magnet currents were plotted absolutely and independently, and the satisfactory continuity of the resulting average curves through these points lend confidence to the general experimental technique, especially to the thermocouple beam monitoring.

It is seen that the number of points is considerably less than the number of energy channels involved. For example, in figure 8 there would be 57 points if every

energy channel was directly plotted. Since the total number of counts accumulated by each channel was quite small, (generally less than 100), and since the inherent uncertainty of the resulting curve is not a sensitive function of the manner in which the counting information is graphically distributed, it was convenient to simply combine channels arbitrarily before plotting. The energy uncertainty of each point on the figures can be inferred from the horizontal spacing of neighboring points. Thus, for instance, while it appears in figure 10 that all curves come together above the high end of the energy axis, this point of view may be deceiving if one considers the horizontal probable error of each point. The most one may safely conclude in consideration of the statistics in this case is that the curves probably fall within a range of 2-4 cross sectional units at, say, 55 Mev.

Data was not shown for energies below about 15 Mev, since it appeared that a different mechanism was responsible for the production of the lower energy γ-rays. At some point between 8 and 12 Mev the yield suddenly increased very greatly with decreasing γ-ray energy, and it was assumed that nuclear excitation was responsible for this effect. Because preliminary studies in this region indicated that the change was quite sudden, it is suggested that further experiments be done to check such characteristics as the structure, cutoff point, and slope of this rapidly rising curve.

(2) Comparison with Previous Work

Wilson's[1] technique consisted in brief of measuring the electron pair energies from pair production in thick lead converters by absorption in a carbon block, and hence the uncertainties in his experimental technique were relatively large. Thus comparison of this work with similar target and beam situations in Wilson's work can at best be an order-of-magnitude comparison. The following experimental results may be compared:

(a) General Spectrum Shape

His spectra from 143 Mev protons on Be, C, and Cu at 90° have roughly the same shape as those presented here, with the outstanding difference that his Z-dependent curves do not diverge at lower energies.

(b) Absolute Cross Sections

In calculating an absolute total cross section, attention must be given to the angular distribution. Although no definite data is now available on the yields at 0° and 180° in the laboratory system, preliminary experiments at these angles have shown that the 0°, 90°, and 180° yields probably do not differ by more than a factor of three. This information, along with the fact that 90° emission is characteristic of a large fraction of solid angle, and the fact that detection at 90° to the beam involves emission from a large angular range of the p-n center-of-mass systems (which move at all angles to the beam) justifies multiplying the 90° differential cross section by 4π to obtain the total cross section. In doing this, then, the

total cross section for the production of γ-rays with greater than 20 Mev energy with 140 Mev protons on Be is $(1.3 \pm .5) \times 10^{-29}$ cm.^{2}, which is in agreement with Wilson's absolute cross section

The relatively large error of $\pm .5 \times 10^{-29}$ cm.^{2} is a result of the counting statistics, lack of precise knowledge of the angular distribution, and uncertainty in such measurements as effective geiger tube areas, vertical scattering loss, etc.

(c) Cross Section Dependence upon Beam Energy for Be

In the present work, the total cross section for γ-ray production above 20 Mev is nearly independent of beam energy, while in Wilson's paper the yield increases with increasing beam energy. Since his estimate of beam current was based largely on indirect deduction instead of direct measurement, one assumes his errors in these deductions could have been large.

(d) Total Cross Section Dependence on Target Material

Both experimental results are in general agreement.

(e) Transformation Calculations

Calculations on the transformation for a $\frac{\sqrt{E_0 - h\nu}}{E_0 h\nu}$ spectrum from the center-of-mass to the laboratory system with both stationary and Fermi gas target nucleons were done for Wilson by J.B. French and P.B. Daitch, and are shown graphically in his paper. These may be compared with their analogues in this work; (see the following section 3).

A numerical comparison shows that while the stationary-nucleon curves agree almost exactly, the moving-nucleon curves disagree by about 25% in some spectral regions. In the stationary-nucleon case they apparently chose 5-10 Mev for the energy picked up by the bombarding proton in the nuclear region. In the present work 8 Mev was chosen. (See the end of appendix 3C for a discussion on this energy gain). The 25% disagreement is most likely due to the choice of momentum distribution; the form of disagreement is such that if both calculations had been done with the same momentum distribution, the agreement would have been much better.

(3) Comparison with Theoretical Predictions

Both the predictions of the phenomenological theory of Ashkin and Marshak[3], and the scalar meson (scalar coupling) theory of Simon[2] give spectra of which the center-of-mass yield is $\frac{\sqrt{E_o - h\nu}}{E_o h\nu}$ for p-n collisions, where E_o is the available energy in the center-of-mass system.

Pseudoscalar meson theory with pseudoscalar coupling (by Simon[2]) gives a $E_o^{\frac{1}{2}} h\nu \sqrt{E_o - h\nu}$ spectrum, which is ruled out by the experimental results of, say, figure 9. It can be shown through consideration of nuclear momentum distribution and proper transformations that the curve shape of figure 9 cannot result from additions of $h\nu \sqrt{E_o - h\nu}$ curve shapes unless perhaps a greater number of extremely low-energy collisions are postulated. This extreme multiple-collision picture is certainly an inconceivable one for Be^9.

In the phenomenological theory[3], Ashkin and Marshak use the quantum electrodynamics, with non-relativistic nucleon motion and the Born approximation, in order to derive expressions for the transition probabilities from initial to final states. The nuclear potential used is the Serber $V(r) = \frac{(1+P_M)}{2} g_i e^{-\lambda r}$, where P_M is the Majorana operator. This potential is found to give a good fit to 90 Mev neutron scattering experiments. Of the six possible spin function transitions, two give rise to magnetic radiation, the other four give rise to electric radiation. The magnetic radiation from spin flip is calculated to be small compared to the electric dipole radiation, and can be neglected. $\frac{d^2\sigma}{d\Omega d\nu}$ for the electric dipole, radiation is given as a complicated function of E_0 and $h\nu$, which can be simplified in the high-energy spectral region to be proportional to $\frac{\sqrt{E_0 - h\nu}}{E_0 h\nu}$. The $\frac{1}{E_0}$ dependence is a reasonable one, since the elastic n-p total scattering cross section varies with E_0 in the same way.

As a first trial in this present work, the center-of-mass $\frac{\sqrt{E_0 - h\nu}}{E_0 h\nu}$ spectra were transformed to the laboratory system for proton laboratory bombarding energies of 38, 100, and 140 Mev; the struck neutrons were considered to be at rest. Figure 12 shows the results. It is apparent that these curves are roughly similar to the corresponding experimental curves of figure 11. A striking difference is the raised position of the 38 Mev experimental curve. The probable explanation is that for 38 Mev protons the single nucleon-nucleon collision picture is not valid, and the

proton-nucleus collision mechanism is mainly responsible for the production of these photons. It is then obvious that the yield would be greater in this case.

The rough agreement of the figure 12 curves with experiment points the way to refinements in calculating the actual laboratory spectral yield from $\frac{\sqrt{E_0 - h\nu}}{E_0 h\nu}$ to compare with experimental results. Appendix (3) outlines the derivation for the calculation to take into account the nuclear motions. In accordance with recent Berkeley experiments, a gaussian with half-width of nuclear momentum density corresponding to 19 Mev kinetic energy was used. It was also assumed that the angular distribution was spherically symmetric in the center-of-mass system; however, it can be shown by the methods of numerical integrations used that the resulting emitted spectrum in the laboratory system would not be markedly influenced by at least a mild departure from this distribution. Because of the use of Simpson's rule for the numerical integrations, it is to be expected that the high-energy tail (say above 80 Mev) may be in error by as much as 25%.

The results of this calculation are shown in figure 13. A comparison is made of this calculation with the experimental result and the previous nucleons-at-rest calculation. The two theoretical curves are normalized at 15 Mev, while the experimental points are scaled to be grouped about the moving-nucleon curve. An absolute determination of the yield from the theory involves some considerable calculation, and has been done for some special cases by the authors; the

results will be presented in a following discussion.

It is seen from figure 13 that in general there is good agreement between theory and experiment. Up to about 75 Mev the curves agree to within the experimental error, while above this energy the theoretical curve is somewhat higher than the experimental one. This discrepancy may result from three sources:

(1) Inadequacy of the gaussian distribution as a representation of nucleon momentum distribution;

(2) Simpson's rule error as previously explained;

(3) Improper choice of curve fitting to the experimental points.

It is of interest to compare the total cross section of experiment with theory. Simon lists some calculations for the field theoretic cases, where the proton laboratory bombarding energy is 180 Mev and the integrations took place between photon energies of 45 and 90 Mev. This should not differ greatly for 140 Mev bombarding energy and a yield between 35 and 70 Mev. The experimentally integrated cross section assumes a spherically symmetric distribution in the center-of-mass. A comparison, between theory and experiment, then shows:

experimentally integrated cross section per neutron: - $(1.2 \pm .5) \times 10^{-30} cm^2$;

scalar meson theory:- - - - - - - - - - $3.0 \times 10^{-30} cm^2$;

pseudoscalar meson theory:- - - - - - - $1.3 \times 10^{-30} cm^2$;

phenomenological theory:- - - - - - - - $1.0 \times 10^{-30} cm^2$;

figure 10 should be examined. As previously explained, it is not to be assumed that the curves are restricted to union at the high-energy end. This is simply what appears to be the most probable set of curves through the experimental points. There are at least two reasonable qualitative explanations, however, for the general merging effect of the high-energy tails.

The most plausible explanation involves consideration of multiple collisions in the p-n collision picture. For a given proton bombarding energy, the mean number of collisions within the nucleus must increase with increasing atomic number of the target material. In the 100 Mev bombarding energy region, the mean energy lost per collision is about 20 Mev[5,6]. Since the probability of bremsstrahlung emission varies approximately inversely with the collision energy, then the lower energy second, third, and fourth collisions have a successively higher probability of contributing to the bremsstrahlung spectrum; and as the atomic number of the target is increased, the mean p-n collision energy will decrease. Because of the $\sqrt{E_o - kv}$ factor, the yield per nucleus at the high-energy end of the spectrum should not increase uniformly with increasing A and/or Z of the target material.

Another explanation or factor which contributes to the merging effect involves the nucleon momentum distribution. If the ratio $\frac{\text{low-momentum components}}{\text{high-momentum components}}$ for the target nucleons was such that this ratio increased with increasing "A", then, for example, the Be high-energy photon

yield would be proportionately larger than for Cu. There is no experimental evidence as yet of the nuclear momentum distribution for the heavier nuclei such as Cu, although one may present some arguments to show that the relative high-momentum components would tend to decrease with increasing A. One argument would consist of making a case for a system of nucleons approaching a Fermi gas (from, say, the near-Gaussian distribution of Be) as the number of nucleons is increased, with the corresponding decrease in the high-momentum components. Another argument would assume a square-well potential, having a radius which increases with increasing A. The wave functions for the various angular momentum states would spread out with the radius, resulting in a narrowing of the corresponding momentum distribution functions.

The rapid divergence of the curves with decreasing photon energy is to be expected because of the multiple-collision effects for heavy nuclei. Second and third collisions within a nucleus (assuming, of course, the p-n collision picture) will be correspondingly less energetic and because of $\frac{\sqrt{E_0 - h\nu}}{E_0 h\nu}$ will contribute a higher ratio of $\frac{\text{low-energy photons}}{\text{high-energy photons}}$ than the first collision.

It is suggested that further experiments be done on hydrogen and deuterium, in order to further check the validity of the $\frac{\sqrt{E_0 - h\nu}}{E_0 h\nu}$ type of spectrum and to examine more carefully the high-energy tail for these simpler cases.

(4) The p+n ⟶ d+γ Reaction

Figures 8, 9, 10 and 11 indicate no "hump" in the spectral region where the photon energy is about one-half the bombarding energy in the laboratory system, to an accuracy determined by the counting statistics in these spectral regions. This is in agreement with Wilson's results. If the reaction was allowed to take place in a field-free region (as opposed to inside a nucleus) then calculations quoted in Wilson's paper indicate that the resulting photon flux should be somewhat greater than the pure p-n collision bremsstrahlung flux in the higher energy spectral region. One must therefore conclude, as does Wilson, that the perturbations of the final reaction states due to the presence of the other nuclear constituents greatly decrease the cross section for the reaction per target neutron. It can be deduced from the experimental results that the reaction cross section per neutron must be decreased by a factor of at least 40 for the beam-target situations here investigated.

In conclusion, then, this experimental work shows that:

(1) the total cross section for Be^9 for the production of photons above 20 Mev energy by 140 Mev protons is $(1.3 \pm .6) \times 10^{-29} cm^2$;

(2) the center-of-mass spectrum shape for p-n collisions is given by $\frac{\sqrt{E_0 - h\nu}}{h\nu}$ with an energy dependence of about $\frac{1}{E_0}$;

(3) the pseudoscalar meson theory with pseudoscalar coupling prediction is inconsistent with experimental results;

(4) the phenomenological theory prediction is consistent with experimental results;

(5) the scalar meson theory with scalar coupling theory prediction is indicated by preliminary experiments to be inconsistent with experimental results only in the angular distribution;

(6) there is no evidence for the reaction $p+n \longrightarrow d+\gamma$.

E. Appendix

(1) Channel Efficiencies Derivation

The following consists of a derivation of the absolute channel counting efficiencies for a beam of photons directed at the converter. The two factors of vertical scattering loss, and loss between effective geiger tube areas are here ignored, hence it is assumed that there is no vertical scattering, and that the geiger tubes form a continuous counting area. The terminology consists of:

d, the converter density;

N_o, Avogadro's number;

A, the atomic weight of the converter material;

h, the converter height;

t, the converter linear thickness;

y, the distance from the converter center along the line of geiger tubes (see figure 15);

y', the distance along the converter;

W, the photon energy;

μ, the ratio of the electron(-) energy (total $\approx$ kinetic energy) to W;

k, a function of the magnetic field strength such that the electron energy equals ky for an orbit through 0 and y (see figure 15);

$\Delta W_{j,k}$, the energy spread or interval of the j'th channel for the same magnetic field setting as is involved in the above k;

I_j, the intensity of the photon beam striking the converter, confined to an energy range $\Delta W_{j,k}$;

I'_j, the number of pairs which are detected per unit time;

j, the general integral designation of the j'th energy channel;

Δy, the distance between geiger tubes = $y_{22} - y_{20} = y_{20} - y_{18}$, etc.;

$\Phi(Z,W,u)du$, the cross section for pair production for a photon of energy W with a fractional splitting of u in an interval du, in a converter with atomic number Z.

The absolute channel efficiency is then $\frac{I'_j}{2y_1 h I_j}$.

It is clear that I'_j is proportional to the converter thickness t, the number of nuclei per unit volume $N_o \frac{d}{A}$, the converter height h, and I_j. In addition, it is proportional to an integral with somewhat involved limits.

To evolve this integral, it is instructive to study pairs originating at y' in the converter in an interval dy', and which are produced by photons in the energy range $\Delta W_{j,k}$ and of energy W appropriate to the j'th energy channel. The integral is built around the cross section $\Phi(W,u)du$;

and the first step is to set the limits in u. An integration over u then gives the total cross section for detected photons for the case of particular photon energy V, originating at y', and the j'th channel. It should be noticed that $\Delta V_{j,k} = 2k \Delta y$ is independent of j. To visualize the limits it is helpful to imagine a line corresponding to V, slid back and forth parallel to y (figure 15) and of length in $y = \frac{V}{2k}$.

For $1 < j \leq 10$:

For $2ky_{j-1} \leq V \leq 2ky_{j+1}$:

the lower limit is $u = \frac{ky_1 - ky'}{V}$;

the upper limit is $u = \frac{V - ky_1 - ky'}{V}$.

For $2ky_{j+1} \leq V \leq 2ky_{j+3}$:

the lower limit is $u = \frac{V - ky_{2j+1} - ky'}{V}$;

the upper limit is $u = \frac{ky_{2j+2} - ky'}{V}$.

For $10 < j \leq 19$:

For $2ky_{j+1} \leq V \leq 2ky_{j+2}$:

the lower limit is $u = \frac{ky_{2j-18} - ky'}{V}$;

the upper limit is $u = \frac{V - ky_{2j-18} - ky'}{V}$.

For $2ky_{j+2} \leq V \leq 2ky_{j+3}$:

the lower limit is $u = \frac{W - ky_{22} - ky'}{W}$;

the upper limit is $u = \frac{ky_{22} - ky'}{W}$.

In addition the resulting Ψ (v) must be suitably weighted for all values of W between $2ky_{j+1}$ and $2ky_{j+3}$. This denotes a second integration with respect to W between the limits $2ky_{j+1}$, $2ky_{j+2}$; and $2ky_{j+2}$, $2ky_{j+3}$; where these integrals are divided by

$$\frac{\Delta W_{j,k}}{2} = 2ky_{j+3} - 2ky_{j+2} = 2ky_{j+2} - 2ky_{j+1}, \text{ etc.,}$$

for proper dimensional and weighting treatment.

Finally, a third integration must be performed over the entire converter by means of the differential dy'.

The results are:

For $j \leq 10$:

absolute channel efficiency =

$$\frac{N_0 \frac{\ell}{2} h I_j t}{2 - y_0 h I_j} \left[\int_{-y_0}^{+y_0} \int_{2dy_{j+1}}^{2dy_{j+3}} \int_{\frac{ky_{22} - ky'}{W}}^{\frac{W - ky_{22} - ky'}{W}} \Psi(W,u)\,du\,dW\,dy' + \right.$$

$$\left. \int_{-y_0}^{+y_0} \int_{2dy_{j+2}}^{2dy_{j+3}} \int_{\frac{W - ky_{22} - ky'}{W}}^{\frac{ky_{22} - ky'}{W}} \Psi(W,u)\,du\,dW\,dy' \right] ;$$

For $j > 10$:

absolute channel efficiency =

$$\frac{N_0 \frac{d}{A} h I_j t}{2y_j h I_j} \left[\int_{-7}^{+7} \int_{2dy_{j+1}}^{2dy_{j+2}} \int_{\frac{W-dy_{j+1}-dy'}{N}}^{\frac{W-dy_{j+2}-dy'}{N}} \Psi(W,u)\,du\,dW\,dy' + \int_{-7}^{+7} \int_{2dy_{j+1}}^{2dy_{j+2}} \int_{\frac{W-dy_{j+1}-dy'}{N}}^{\frac{W-dy_{j+2}-dy'}{N}} \Psi(W,u)\,du\,dW\,dy' \right].$$

Unfortunately $\Psi(W,u)$ as expressed in the usual literature is not an integrable function, and methods for numerical approximations must be found. The simplest and most useful of such approximations consist of:

(a) considering the splitting curves as flat, so that Ψ is no longer a function of u;

(b) choosing a mean value of W for each channel ($W = 2ky_{j+2}$) so that Ψ is a constant for each channel.

The second approximation is a good one since does not vary rapidly over the relatively small range of $\Delta W_{j,k}$; the first can be shown to be an adequate approximation (to within several %) if Ψ is properly chosen for each channel. As explained in 4(b), Ψ was chosen to correspond to $u = .3 = .7$. Henceforth Ψ may be designated by Ψ_j, so that for the j'th channel Ψ_j is evaluated at the mean energy $W = 2ky_{j+2}$. With these approximations, then,

for $1 \leq j \leq 10$:

absolute channel efficiency =

$$\frac{N_0 \frac{f}{A} t \, F_j}{\pi y_i \frac{\Delta W_{i,A}}{2}} \left[\int_{-\gamma_i}^{+\gamma_i} \int_{\Delta y_{i,0}}^{\Delta y_{i,1}} \left(1 - \frac{\pi \Delta y_i}{W}\right) dW dy' + \int_{-\gamma_i}^{+\gamma_i} \int_{\Delta y_{i,0}}^{\Delta y_{i,j-1}} \left(\frac{\pi \Delta y_{i,(j-1)}}{W} - 1\right) dW dy' \right] =$$

(by using the first term of the ln expansion)

$$\frac{N_0 \frac{f}{A} t \, F_j \, (\Delta y)}{\frac{\Delta W_{i,A}}{2}} \left[\frac{y_{i,0} - y_i}{y_{i,0}}\right] = \frac{F_{i,j}}{y_{i,0}} \left(\Delta y \, N_0 \frac{f}{A} t\right);$$

and for $10 \leq j \leq 19$, using similar procedures:

absolute channel efficiency =

$$F_j \frac{(2o-j)}{y_{i,0}} \left(\Delta y \, N_0 \frac{f}{A} t\right).$$

These were the approximations used in the actual computations.

(2) Vertical Scattering

Let it be assumed that all electrons originate on a vertical line of the converter, and let the previously circular electron orbits be "unrolled" to straight lines. Referring then to figure 16 let the x axis be the vertical converter line, and the y axis the line of [illegible] in a horizontal plane. This latter axis is linear in electron kinetic energy, to a good approximation.

Considering electrons of a particular energy E' which terminate on a vertical line through y', it is seen that two special orbits of this energy electron are r_1 and r_2, which make angles θ_1 and θ_2 with the horizontal. Any electron of energy E' is "lost" if its angle with the horizontal is so great that it meets the y axis at a distance smaller than y', and therefore θ_1 and θ_2 are two critical angles.

Now for a beam of photons passing through the line converter one may define a line density of electrons $\eta(E,x)$ which leave the converter in the forward direction. This density must be of such a form that $\eta(E,x) = f(E)X(x)$, where f and X are functions at this point undefined. This is so because the distance from the cyclotron target will be great enough so that the photon energy distribution will not change over the space of the converter.

The object of the following calculation is to find what fraction of electrons of energy E' are "lost" through vertical scattering.

The Rossi-Greisen paper[12] deals in part with the scattering of electrons through thin foils, and it is shown that for a pencil of electrons of kinetic energy E (in Mev) passing through a converter of radiation length thickness t

$$G(E,t,\theta)d\theta = \frac{E}{\theta_0^2 t}\, e^{-\frac{\theta^2}{\theta_0^2 t}}\, d\theta \quad ,$$

where $G(E,t,\theta)d\theta$ is the probability of an outgoing electron

being scattered into the range $d\theta$ at an angle in radians of θ with the forward direction. But for the case here dealt with, that is, pair electrons uniformly created throughout the converter, this distribution function becomes

$$F(\epsilon, t, \theta) = N \left[\int_0^t \frac{E}{\sqrt{\epsilon'}} e^{\frac{\epsilon' \theta'}{\sqrt{\epsilon'} t'}} dt' \right] d\theta ,$$

where N is determined by the normalization,

$$N \int_{-\infty}^{+\infty} \int_0^t \frac{E}{\sqrt{\epsilon'}} e^{-\frac{\epsilon' \theta'}{\sqrt{\epsilon'} t'}} dt' d\theta = 1 ;$$

so that $N = \frac{1}{E\sqrt{\pi}}$ and

$$F(E, t, \theta) = \frac{1}{E\sqrt{\pi}} \int_0^t \frac{E}{\sqrt{\epsilon'}} e^{-\frac{\epsilon' \theta'}{\sqrt{\epsilon'} t'}} dt' .$$

Now if one assumes that the critical angle for any point x of the converter is given by $\frac{x}{y}$, (so that $\tan \frac{x}{y} = \frac{x}{y}$,) for loss at the bottom, then for any element dx at x the total number of electrons lost at the bottom is given by

$$\int_{\theta = \frac{x}{y}}^{\theta = \frac{x}{t}} \eta(\epsilon'; x) F(\epsilon'; t, \theta) d\theta dx .$$

Thus the fraction of electrons of energy E' which are lost from the entire converter to both top and bottom is given by

$$\frac{2\int_{x_1}^{x_2}\int_{\alpha/y}^{\pi/2}\eta(E';x)\,F(E';t,\theta)\,d\theta\,dx}{\int_{x_1}^{x_2}\eta(E';x)\,dx} =$$

$$\frac{2\int_{x_1}^{x_2}\int_{\frac{A}{E'k(I)}}^{\pi}\int_{0}^{t}\frac{\chi(x)}{t'\sqrt{\pi\alpha}}\frac{E'}{Vc'}\,e^{-\frac{E'^2\theta^2}{V\alpha t'}}\,dt'\,d\theta\,dx}{\int_{x_1}^{x_2}\chi(x)\,dx};$$

where y' has been replaced by k(I) E', k(I) being a function of the magnet current only.

It can now be shown that this fraction is independent of the orbit energy E'.

From the first integration in the above integral it is seen that θ always appears as $E'^2\theta^2$, so that $F(E',t,\theta)$ may be written as $E'F'(E'\theta,t)$, and the integral may be written as :

fraction lost =

$$2\int_{x_1}^{x_2}\int_{\frac{A}{E'k(x)}}^{\pi_1}\frac{\chi(x)\,E'\,F'(E'\theta,t)\,d\theta\,dx}{t\sqrt{V\alpha\pi}} =$$

$$\frac{2\int_{x_1}^{x_4}\int_{\theta_2}^{\infty}\frac{\chi(x)\,F'(E'\theta,t)}{t\sqrt{\pi\theta}}\,d(E'\theta)\,dx}{\int_{x_1}^{x_4}\chi(x)\,dx};$$

in which the limits of the first integration have been changed according to the new variable of integration. The use of ∞ in the new upper limit is justified because of the form of $F'(E'\Phi,t)$ which contains a gaussian function; and for thin foils this gaussian is vanishingly small at $\Phi = \frac{E}{E'}$ or $E'\Phi = E$.

This last integral expression for the fraction of electrons lost by vertical scattering is independent of E'.

The derivation contains two assumptions which demand further comment.

The first assumption is that the electrons originate on a vertical line, instead of an actual areal converter. But the derived fraction is independent of y, hence it must be valid for any vertical line converter on the y axis, and hence for an actual areal converter.

The second assumption is that $\tan\frac{x}{y} = \frac{x}{y}$, or that the mean scattering angle is quite small. This implies that the derived results are only true to first order. The second order distortion may be minimized by using thin converters and/or converters of narrow height.

(3) Calculation of Laboratory Spectrum for 140 Mev Protons using a Nuclear Momentum Distribution

Assumptions:

(a) There is at most one nuclear collision per proton. This is justifiable on mean free path considerations.

(b) The spectrum in the center-of-mass system depends on the photon energy $(h\nu)_o$, and the available energy E_o, by means of $\frac{\sqrt{E_o - (h\nu)_o}}{4(h\nu)_o}$, where the subscript o refers to the center-of-mass system

(c) The photons are emitted with spherical symmetry in the center-of-mass system.

(d) The target nucleons are considered as a gas inside the nuclear potential well, and in order to interact with the neutrons of the nucleus the bombarding protons must enter the well and pick up some 8 Mev in available reaction energy. This is in accordance with recent nucleon-nucleon calculations for this energy range.[9]

(e) The momentum distribution of the target neutrons is assumed to be a gaussian in accordance with recent Berkeley experiments[x], such that the probability that a neutron have a momentum p in a range dp is given by $Ne^{-\frac{p^2}{p_F^2}}dp$

---

x These results are given in a number of 1953-1954 UCRL reports, among them J.H. Wilcox, UCRL-2540, 1953 (unpublished).

where p is the neutron momentum corresponding to 10 Mev kinetic energy, and N is the proper normalizing constant.

(f) The neutron motions are treated non-relativistically.

Terminology:

Let the subscript o refer only to quantities measured in the center-of-mass system.

ϕ is the angle of photon emission with respect to the direction of the center-of-mass motion;

θ is the angle made by a target neutron with respect to the beam direction before collision; (the "latitude", with the north pole pointing in the beam direction);

x,y,z represent laboratory cartesian axes such that x is upward, y is toward the pair spectrometer, z is in the beam direction, and the origin is imagined as fixed in the target nucleus;

μ is the angle of "longitude" as measured upward from the y direction for a target neutron;

$\vec{V}$ is the velocity vector of the center-of-mass system in the reference frame of x,y,z; with magnitude V, along with the usual terminology of

$\vec{\beta} = \frac{\vec{V}}{c}$, and

$\beta = \frac{V}{c}$, and

$\gamma = \frac{1}{\sqrt{1-\beta^2}}$;

n and p as subscripts refer to target neutron and bombarding proton;

$\mathcal{E}$ is the total energy of a nucleon;

E is the kinetic energy of a nucleon or system of nucleons;

p is the momentum of a nucleon;

I is the proton beam intensity;

$N_t \frac{A}{B} \ell$ is the number of nuclei per unit area of target.

General Procedure

The experiments here described measured the cross section for photon emission per nucleus per unit solid angle per 1 Mev energy interval. This, then, will be the quantity which will be theoretically calculated in the following work. The method used will consist of these steps:

(a) Finding β , γ, and $E_n + E_p$ of the center-of-mass system, which is composed of a bombarding proton and a target neutron; because of the neutron motions this system will in general not move along the beam direction.

(b) Finding the relativistic transformation for $\frac{d^2\sigma}{d\Omega_c dW_c}$ into the laboratory $\frac{d^2\sigma}{d\Omega dW}$ as a function of β, γ , and $E_0 = E_{no} + E_p$.

(c) Completing the transformation having found $\vec{\beta}$ and γ in step (a).

(a) The center-of-mass system:

The following relationships are given from the mechanics of special relativity:

(1) $\mathcal{E}_{p'} = \gamma (\mathcal{E}_p - \vec{V} \cdot \vec{p}_p)$;

(2) $\vec{V} = \frac{(\vec{p}_+ + \vec{p}_-)c^2}{\mathcal{E}_- + \mathcal{E}_p}$;

(3) $E_{p'} = \mathcal{E}_{p'} - m_p c^2$;

and by substituting (2) into (1), then (1) into (3),

(4) $E_{p'} = \gamma \left[E_p + m_p c^2 - \frac{m_p c^2}{\gamma} - \frac{(\vec{p}_+ + \vec{p}_-) c^2 \cdot \vec{p}_p}{\mathcal{E}_- + \mathcal{E}_p} \right]$.

But since this is a case of two nucleons of equal mass, the total available kinetic energy

$E_0 = E_{p'} + E_{n'} = 2 E_{p'}$ and

(5) $E_0 = 2\gamma \left[E_p + m_p c^2 - \frac{m_p c^2}{\gamma} - \frac{(\vec{p}_- + \vec{p}_-) c^2 \cdot \vec{p}_p}{\mathcal{E}_- + \mathcal{E}_p} \right]$;

or more conveniently

(5') $E_0 =$

$$2\gamma \left[\mathcal{E}_p + m_p c^2 - m_p c^2 - \frac{\mathcal{E}_p^2 - m_p^2 c^4 + \sqrt{(\mathcal{E}_p^2 - m_p^2 c^4)(2 m_n c^2 E_-)} \cos\theta}{2 m_n c^2 + \mathcal{E}_p + E_-} \right].$$

Using the definition of γ , and (2)

(6)

$$\gamma = \frac{1}{\sqrt{1 - \frac{\mathcal{E}_p^2 - m_p^2 c^4 + 2 m_n c^2 E_- + 2\sqrt{(\mathcal{E}_p^2 - m_p^2 c^4)(2 m_n c^2 E_-)} \cos\theta}{(2 m_n c^2 + \mathcal{E}_p + E_-)^2}}}$$

The magnitude of $\vec{\beta}$ is given from (2) to be

(7)

$$\beta = \frac{\sqrt{E_p^2 - m_0^2c^4 + 2m_0c^2E_- + 2\left(\sqrt{E_p^2 - m_0^2c^4}\right)\left(\sqrt{2m_0c^2E_-}\cos\theta\right)}}{2m_0c^2 + E_p + E_-} ,$$

and from (2) and definitions of Θ, μ

(8)

$$\beta_y = \frac{P_{my}c}{E_- + E_p} = \frac{\sqrt{2m_0c^2E_-}\sin\theta\cos\mu}{2m_0c^2 + E_p + E_-} .$$

(b) Finding the transformation:

The quantity to be transformed is

(9) $\dfrac{d^2\tau}{d\Omega_0 dW_0} \equiv \dfrac{d^2\tau}{d\Omega_0 d(h\nu)_0} = \dfrac{A}{I_0 \mu_0 \ell} \dfrac{d^2m}{d\Omega_0 dW_0}$ where

(10) $\dfrac{d^2m}{d\Omega_0 dW_0} = \dfrac{K''\sqrt{E_0 - (h\nu)_0}}{E_0(h\nu)_0}$; $W \equiv h\nu$;

in which n represents the number of photons, and K'' represents a constant containing the necessary fundamental constants for correct dimensional expression. I_0 must here be a constant because of the methods used in finding the experimental ordinates, which consisted in part of dividing by an effective proton beam current and neglecting any such concept as nucleon motion. For the nucleon-nucleon system concept here used, this variation of effective current with center-of-mass motion will be taken into account as the calculation progresses.

Substituting (10) into (9) results in

(11) $\frac{d^2\sigma}{d\Omega_o dW_o} = \frac{K'\sqrt{E_o-(h\nu)_o}}{E_o(h\nu)_o}$ where

(12) $K' = \frac{\square''\Lambda}{I_o''_o\, td}$.

Now the relativistic energy and angle transformations yield

(13) $(h\nu)_o = (h\nu)\gamma(1-\beta\cos\phi)$

and

(14) $dW_o \equiv d(h\nu)_o = d(h\nu)\,\gamma(1-\beta\cos\phi)$;

(15) $\cos\phi = \frac{\cos\theta_o+\beta}{1+\beta\cos\theta_o}$, from which

(16) $d\Omega_o = \frac{d\Omega}{\gamma^2(1-\beta\cos\phi)^2}$.

Substituting (13), (14), and (16) into (11), (11) becomes

(17) $\frac{d\sigma}{d\Omega\, dW} = \frac{K'}{\gamma^3(1-\beta\cos\phi)^3}\,\frac{\sqrt{E_o-(h\nu)\gamma(1-\beta\cos\phi)}}{E_o h\nu}$

E_o, of course, is not to be transformed since it is the energy available for photon emission, and is invariant.

For a pair spectrometer set up at 90° to the proton beam

(18) $\phi = \frac{\pi}{2} - \sin^{-1}\frac{\beta_z}{\beta}$ and

(19) $\cos\phi = \frac{\beta_z}{\beta}$;

substitution of (19) into (17) yields

$$(20) \qquad \frac{d^2\sigma}{d\Omega\, dW} \propto \frac{K'}{\gamma^2(1-\beta_z)^3} \frac{\sqrt{E_0-(h\nu)\gamma(1-\beta_z)^2}}{E_0(h\nu)} .$$

(c) Completing the derivation:

The probability that a target neutron will have a direction θ, u in a range $d\theta$, du is proportional to $d\theta \frac{d}{du}$, since the nucleon situation is assumed to be one of spherical symmetry. Furthermore, as previously mentioned, the momentum distribution assumed is a gaussian one, and the probability that a target neutron have an energy E_n in a range dE_n is given by $N e^{-\frac{E_n}{T}} \sqrt{E_n}\, dE_n$.

There is one more weighting factor to be dealt with. This is the relative number of collisions per unit time, as a function of E_n, Θ, and μ. As an example, it is clear that for target neutrons moving in the -Z direction there are more collisions per unit time than for neutrons moving in the Z direction; and so a term which is proportional to the relative velocity between proton and neutron must be inserted as a weighting factor.

The relative velocity is proportional to

$$\sqrt{E_0+E_n-2\sqrt{E_0 E_n}\cos\theta}$$

in the laboratory system.

The result sought for is then

(21) $$\frac{d^2\sigma}{d\Omega\, d\omega} =$$

$$K \int_0^{2\pi} \int_0^{\nu} \int_0^{\infty} \frac{\ell^{-\frac{E_\pi}{E_0}} \sqrt{E_\pi (E_p + E_n - 2\sqrt{E_p E_n}\cos\theta)(E_n - h\nu + h\nu(1-\beta_y))}}{\gamma^3 (1-\beta_y)^3 E_n h\nu} dE_\pi\, d\theta\, d\phi,$$

where all the constants of proportionality have been included in the new constant K. By substituting (5'), (6), and (8) into (21) the entire integrand becomes a function of only E_π, θ, and μ, and is numerically integrable.

Since E_π appears in units of Mev in $\ell^{-\frac{E_\pi}{E_0}}$, then E_0, $h\nu$, m_0c^2, and E_p must also be expressed in these units.

Some thought must be given to the numerical value for E_p because of the concept of the nuclear potential well. It has been the fashion in recent years[6,9] to assume that the concept of the nuclear potential well is applicable to high-energy bombardments, and that bombarding nucleons pick up some 30 Mev in the center-of-mass system in entering the nuclear region. While the concept of the "30 Mev" potential well is a useful one for low-energy nuclear phenomena such as energy-level structure, low-energy p-n interactions, etc., there is no published experimental evidence for bombarding energies of 100 Mev and greater showing that such a "30 Mev" well exists. It cannot be detected and measured in high energy bombardments such as nucleon-nucleon

scattering, for the effect of the well "cancels out". Indeed, one may present some simple arguments to show that it may be unwise to add this 30 Mev. In a classical type of argument one may say that for, say, 100 Mev protons on Be the bombarding protons suffer only about one collision within a nucleus and do not strongly interact with the other nucleons within the same nucleus. The concept of the "30 Mev well" is intimately tied in with nuclear interactions which are strong and full, such as the bound nuclear states.

Very recent work on the new Teller model at this laboratory indicates that for high-energy bombardments (100 Mev and greater) the bombarding nucleons should experience forces which are appropriate to potential wells which are shallower than 30 Mev, perhaps by a large factor.

In this present work the conservative choice of about 5 Mev was made for the energy picked up by the 140 Mev protons in the nuclear region, in the center-of-mass system; this 5 Mev was carried into the transformation calculations, both with and without nucleon motion.

F. Acknowledgments

The author would like to express his sincere thanks and gratitude to Professor D.J. Hoyer for his guidance, encouragement, and help in the many phases of this research. Many thanks are also due to colleagues Harlan Shaw and Charles Waddell for their long and continued help and contributions as part of the research team which designed the equipment, spent some two years in experimentation, and analyzed the data.

Sincere acknowledgments are to be given to Dr. Walter E. Crandall for his guidance in many phases of the project, to James Vale and Lloyd Hauser for their help in organizing and maintaining the runs, and to the cyclotron crew, the maintenance men, and the many other divisions of the laboratory who contributed directly or indirectly to the success of this project.

Special thanks are given to the author's wife for her invaluable help in performing numerical integrations, typing the manuscript, and giving a great deal of encouragement along the way.

G. References

1. R. Wilson, Phys. Rev. 85, 563 (1952).
2. A. Simon, Phys. Rev. 70, 573 (1950).
3. J. Ashkin and R.E. Marshak, Phys. Rev. 76, 58 (1949).
4. B. Kursunoglu, Phys. Rev. 98, 1156 (1955).
5. R. Serber, Phys. Rev. 72, 1114 (1947).
6. M.L. Goldberger, Phys. Rev. 74, 1269 (1948).
7. Bernardini, Booth, and Lindenbaum, Phys. Rev. 88, 1017(1952).
8. S.G. Rudstam, Phil. Mag. 44, 1131 (1953).
9. J.W. Meadows, Phys. Rev. 98, 744 (1955).
10. D. Halliday, "Intro. Nucl. Phys.", J. Wiley and Sons, (1950).
11. W.R. Crandall and B.J. Moyer, Phys. Rev. 92, 749 (1953).
12. B. Rossi and K. Greisen, Rev. Mod. Phys. 13, 240 (1941.
13. C.R. Emigh, Phys. Rev. 86, 1023 (1952).
14. J. Wheeler and W. Lamb, Phys. Rev. 55, 858 (1939).
15. R. Walker and B. McDaniel, Phys. Rev. 74, 315 (1948).

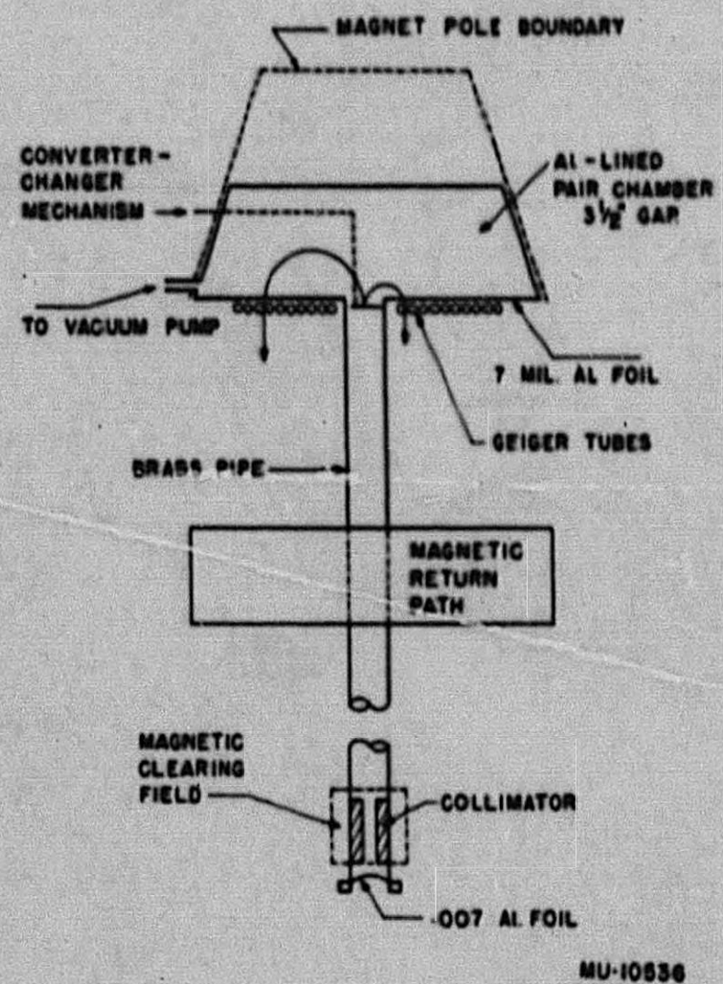
MAGNET POLE BOUNDARY
CONVERTER-CHANGER MECHANISM
Al-LINED PAIR CHAMBER 3½" GAP
TO VACUUM PUMP
7 MIL Al FOIL
GEIGER TUBES
BRASS PIPE
MAGNETIC RETURN PATH
MAGNETIC CLEARING FIELD
COLLIMATOR
.007 Al FOIL
MU-10536

Fig. 1.

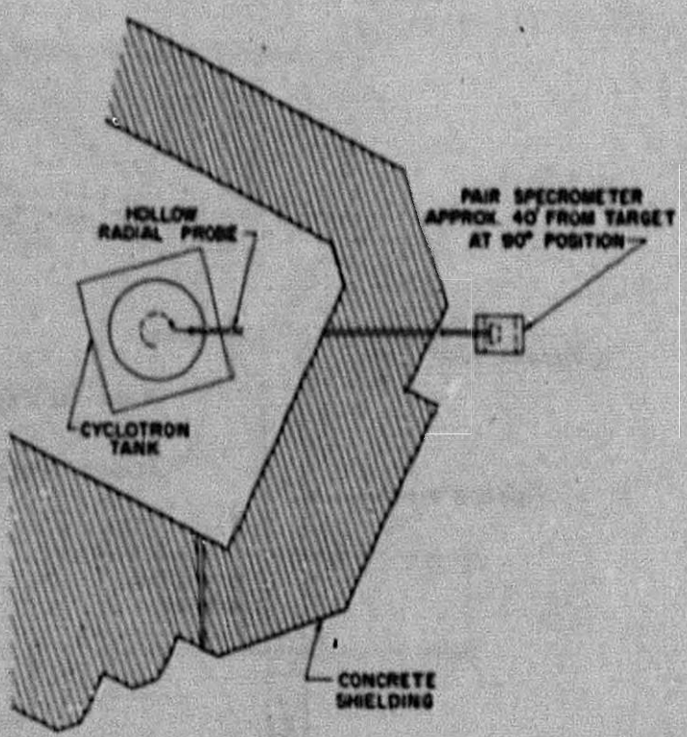
PAIR SPECROMETER
APPROX. 40° FROM TARGET
AT 90° POSITION
HOLLOW
RADIAL PROBE
CYCLOTRON
TANK
CONCRETE
SHIELDING
MU-10537

Fig. 2.

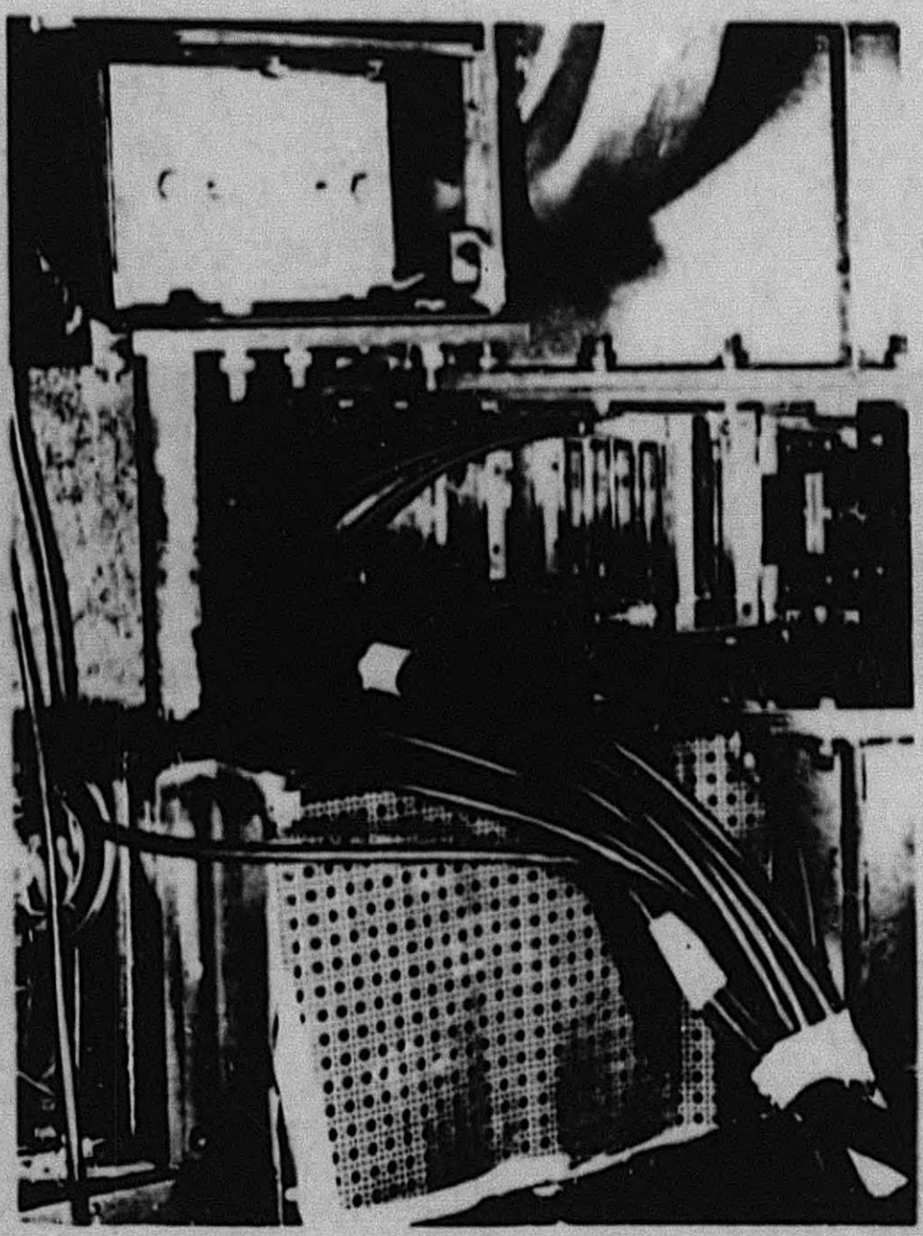

ZN-1408

Fig. 3

ZN-1409

Fig. 4

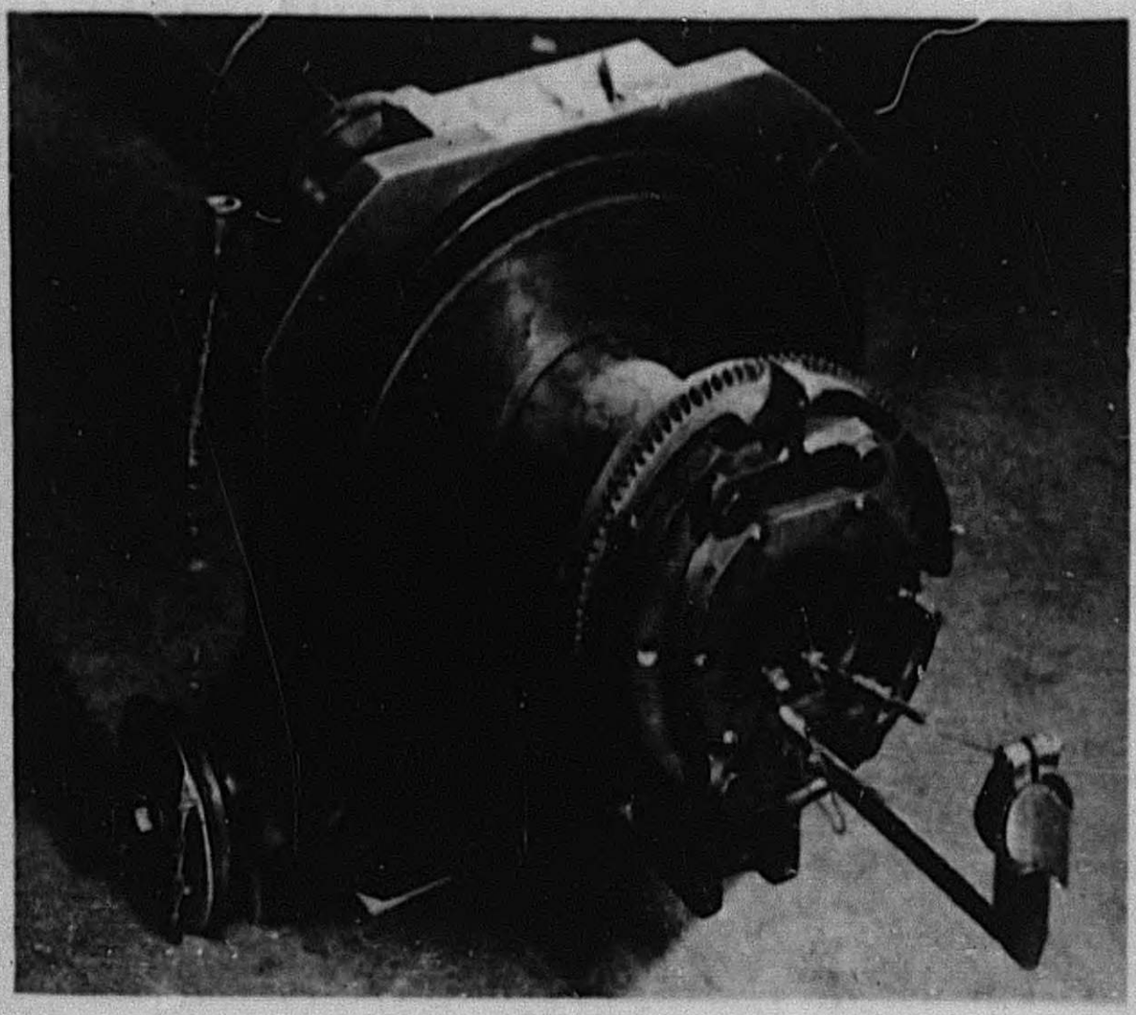

ZN-1410

Fig. 5

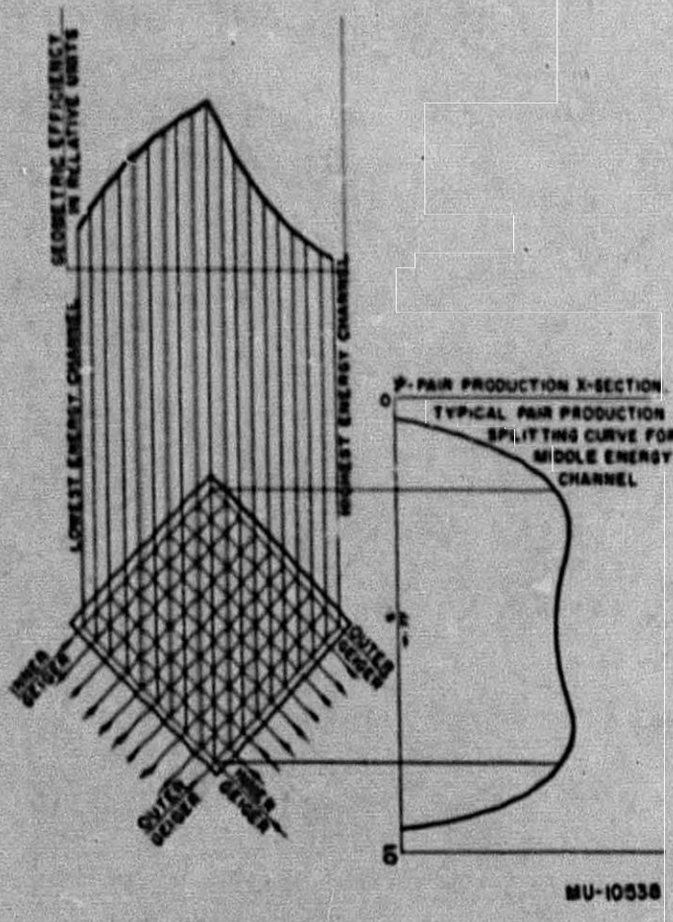
LOWEST ENERGY CHANNEL
HIGHEST ENERGY CHANNEL
INNER DETECTOR
OUTER DETECTOR
OUTER DETECTOR
INNER DETECTOR
P - PAIR PRODUCTION X-SECTION
TYPICAL PAIR PRODUCTION SPLITTING CURVE FOR MIDDLE ENERGY CHANNEL
0
1/2
1
MU-10538

Fig. 6.

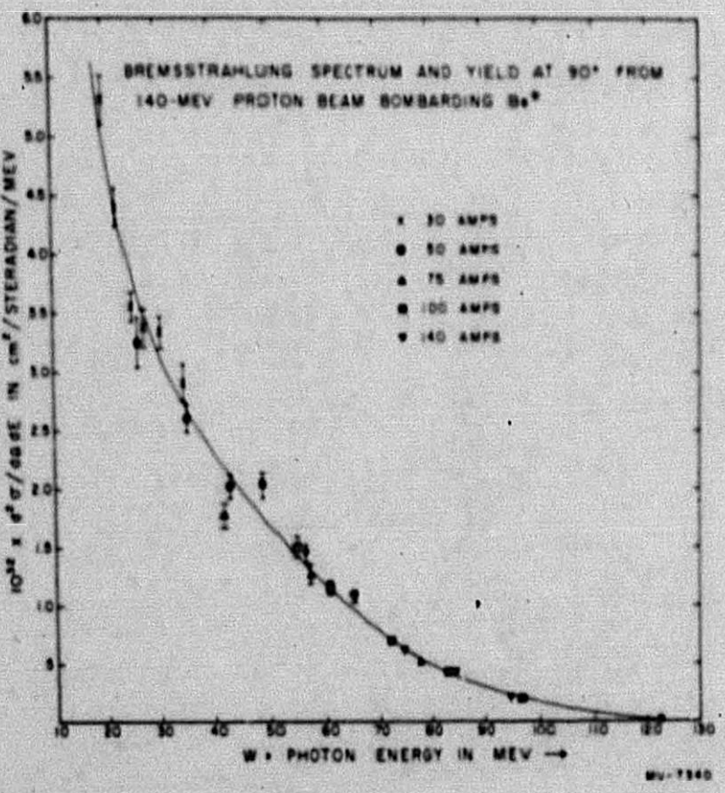
BREMSSTRAHLUNG SPECTRUM AND YIELD AT 90° FROM
140-MEV PROTON BEAM BOMBARDING Be*
x 50 AMPS
● 50 AMPS
▲ 75 AMPS
■ 100 AMPS
▼ 140 AMPS
10 20 30 40 50 60 70 80 90 100 110 120 130
W = PHOTON ENERGY IN MEV →
BU-7340

Fig. 9.

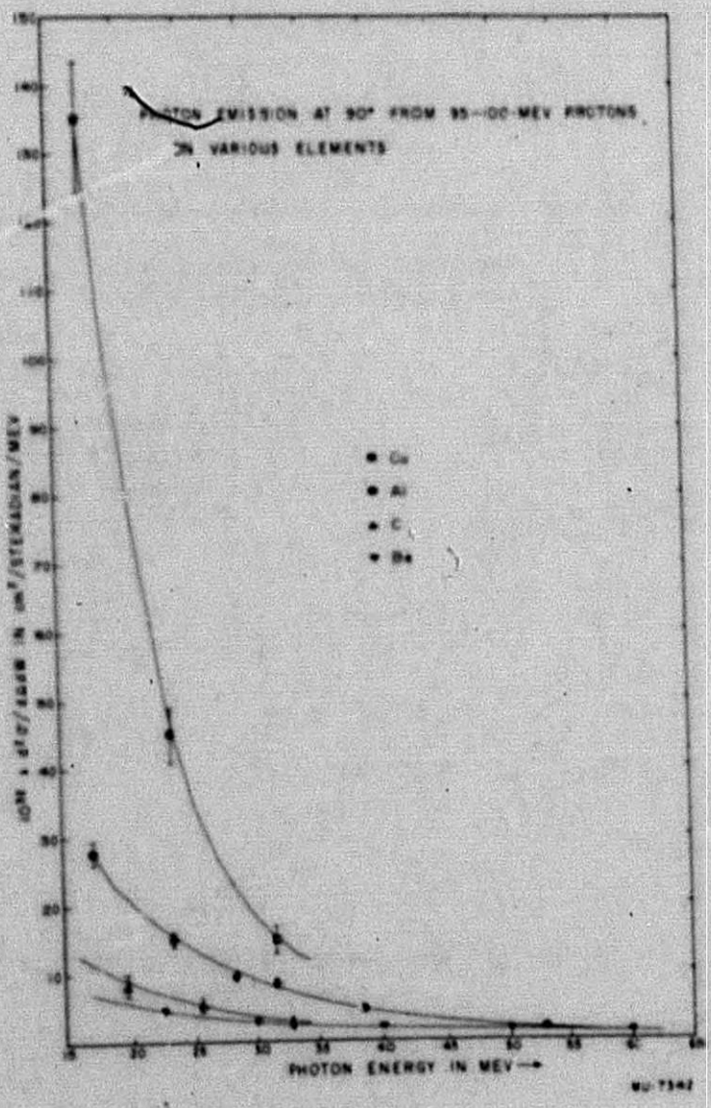
PHOTON EMISSION AT 90° FROM 95-100 MEV PROTONS
ON VARIOUS ELEMENTS
Cu
Al
C
Be
PHOTON ENERGY IN MEV
WU-7342

Fig. 10.

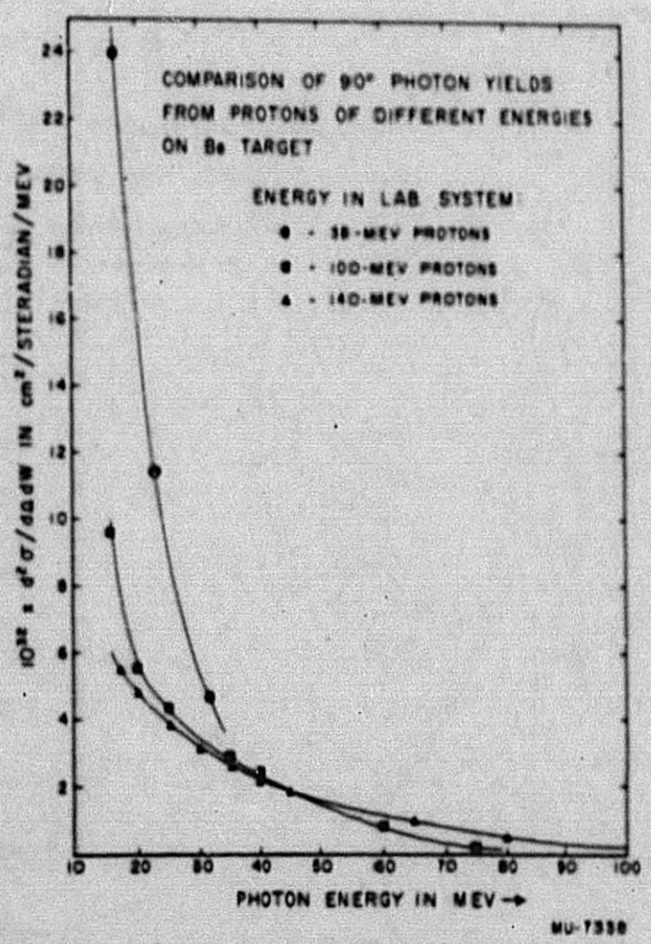

Fig. 11.

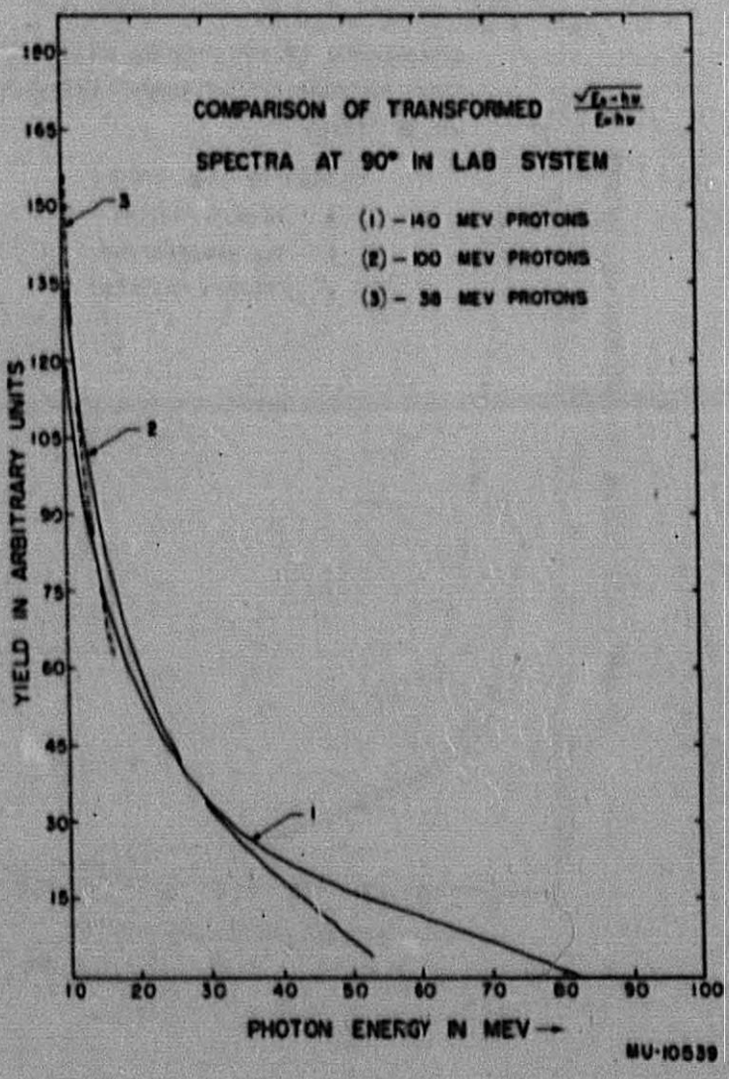
COMPARISON OF TRANSFORMED $\frac{\sqrt{E_0 - h\nu}}{E_0 h\nu}$
SPECTRA AT 90° IN LAB SYSTEM
(1) – 140 MEV PROTONS
(2) – 100 MEV PROTONS
(3) – 38 MEV PROTONS
YIELD IN ARBITRARY UNITS
PHOTON ENERGY IN MEV →
MU-10539

Fig. 12.

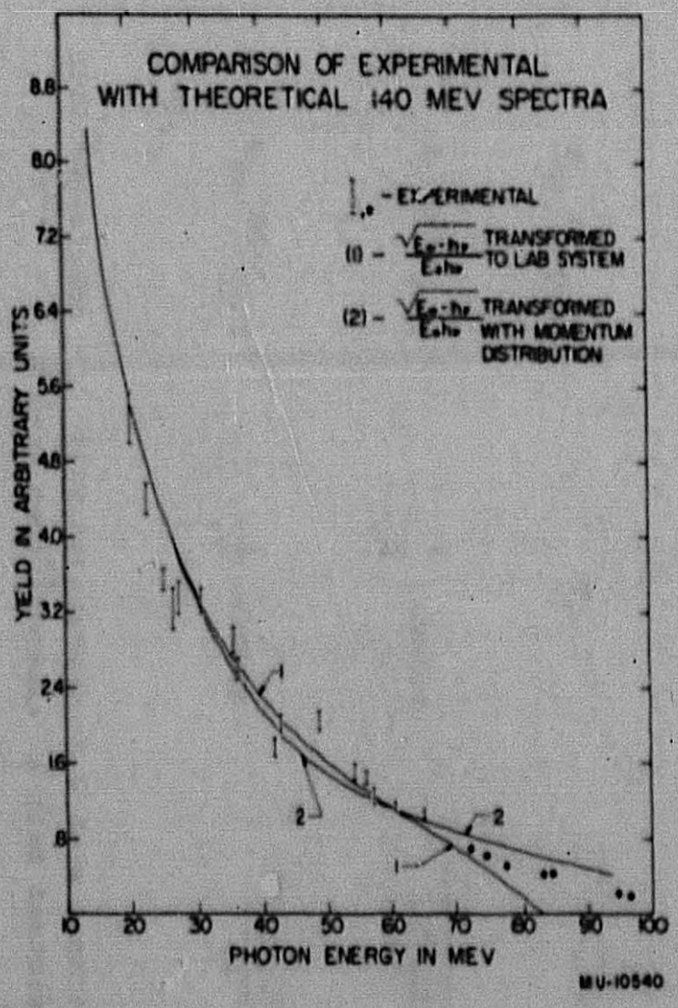
COMPARISON OF EXPERIMENTAL
WITH THEORETICAL 140 MEV SPECTRA
- EXPERIMENTAL
(1) - TRANSFORMED TO LAB SYSTEM
(2) - TRANSFORMED WITH MOMENTUM DISTRIBUTION
YELD IN ARBITRARY UNITS
PHOTON ENERGY IN MEV
MU-10540

Fig. 13.

Source	Spectrum shape in C.M.	Dependence on proton energy	Integrated Cross-section per neutron; 35-70 Mev	Angular Distribution in C.M.
1- pseudoscalar theory with pseudoscalar coupling - Brueckner	$h\nu\sqrt{E_o - h\nu}$	E_o^2	1×10^{-30} cm^2	small departure from spherical symmetry
2- scalar theory with scalar coupling - Simon	$\frac{\sqrt{E_o - h\nu}}{h\nu}$	approx. $\frac{1}{E_o}$	3×10^{-30} cm^2	large departure from spherical symmetry
3- phenomenological theory - Ashkin and Marshak	$\frac{\sqrt{E_o - h\nu}}{h\nu}$	approx. $\frac{1}{E_o}$	1×10^{-30} cm^2	small departure from spherical symmetry
Experimental	consistent with 2,3 inconsistent with 1	consistent with 2,3 inconsistent with 1	consistent with 1,2,3	consistent with 3, inconsistent with 1,2 (preliminary results)

FIGURE 14. TABULAR COMPARISON BETWEEN THEORETICAL PREDICTIONS AND EXPERIMENTAL RESULTS

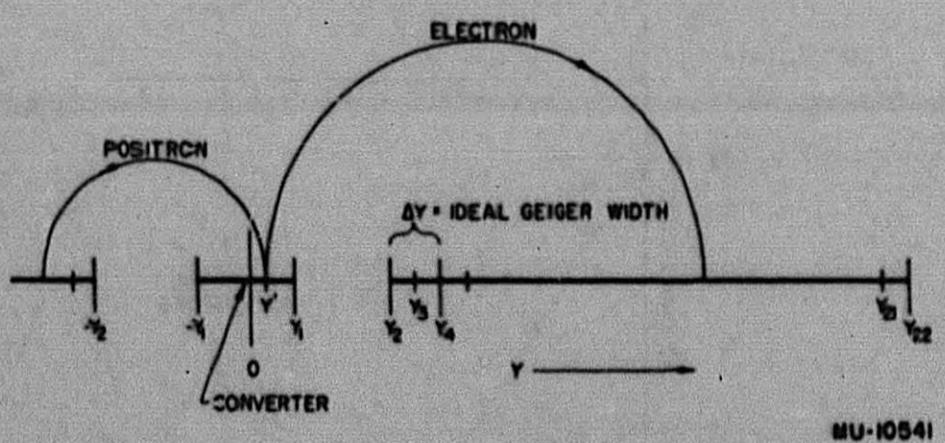
ELECTRON
POSITRON
ΔY = IDEAL GEIGER WIDTH
CONVERTER
Y
MU-10541

Fig. 15.

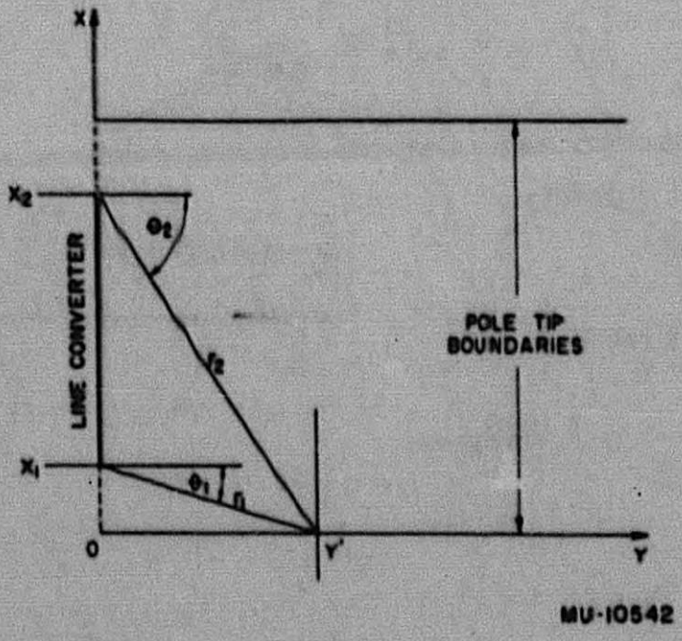

Fig. 16.